Supporting Information

Nitrogen-doped carbon integrated nickel-cobalt metal phosphide marigold flowers as a high capacity electrode for hybrid supercapacitors

Pragati A. Shinde[a], Muhammad Farooq Khan[b], Malik A. Rehman[a], Euigeol Jung[a], Quang N. Pham[c], Yoonjin Won[c], Seong Chan Jun[a]**

[a] Nano-Electro Mechanical Device Laboratory, School of Mechanical Engineering, Yonsei University, Seoul 120-749, South Korea

[b] Department of Electrical Engineering, Sejong University, 209 Neungdong-ro, Gwangjin-gu, South Korea

[c] Department of Mechanical and Aerospace Engineering, 4200 Engineering Gateway, University of California, Irvine, Irvine, CA 92697–2700, USA

Corresponding Author

*Prof. Seong Chan Jun

E-mail: scj@yonsei.ac.kr, Fax: +82-2-312-2159, Tel: +82-2-2123-5817.

*Prof. Yoonjin Won

E-mail: won@uci.edu

Supporting Information 1

Experimental section

Chemicals

All chemical reagents and solvents were analytical grade and used as received without further purification. Nickel nitrate hexahydrate ($Ni(NO_3)_2.6H_2O$), cobalt nitrate hexahydrate ($Co(NO_3)_2.\ 6H_2O$), 2-amino-1,4-benzenedicarboxlic acid (aminoterephthalic acid), N,N dimethylformamide (DMF), sodium hypophosphite ($NaH_2PO_2.H_2O$), potassium hydroxide (KOH) and ethanol were purchased from Sigma-Aldrich.

Synthesis of Ni-Co-MOFs

In a typical synthesis, $Ni(NO_3)_2.6H_2O$ (0.05 M), $Co(NO_3)_2.6H_2O$ (0.05 M) and 0.366 g of aminoterephthalic acid were dissolved in a mixture of 35 mL of DMF and ethanol (V_{DMF}:$V_{ethanol}$ = 7:1) with the assistance of constant stirring for 10 min. Then, the precursor solution was poured into the Teflon-lined stainless steel autoclave. The well cleaned Ni-foam was inserted into the Teflon-liner and the autoclave was maintained at 140 °C for 12 h in an oven. After the autoclave naturally cooled down to room temperature, the Ni-foam coated with precursor material was removed and washed several times with ethanol and DI water. Finally, the Ni-foam coated with purple color products were obtained after drying at 60 °C overnight. The mass loading of the deposited material is calculated by taking the mass difference of the substrate before and after deposition of the active material. The calculated mass loading of the Ni-Co-MOFs over the Ni-foam current collector in 1 cm^{-1} is 2.8 mg cm^{-2}.

Synthesis of Ni-Co/NC nanostructures

The Ni-Co/NC nanostructures were prepared according to the following procedure. The Ni-foam with previously deposited Ni-Co-MOFs was heat treated in a tube furnace under at

600°C for 2 h under Ar atmosphere with the heating rate of 2 °C min^{-1}. It was then naturally cooled to the room temperature. The Ni-foam coated with black color products was obtained. After that the resultant samples were transferred for the phosphorization.

Synthesis of NiCoP/NC nanostructures

The NiCoP/NC nanostructures were prepared by the one-step phosphorization of Ni-Co/NC. To prepare NiCoP/NC nanostructures, two-zone tube furnace was used. The quartz boat with Ni-Co/NC coated Ni-foam and $NaH_2PO_2.H_2O$ (0.3 g) were placed separately, with $NaH_2PO_2.H_2O$ at the upstream side of a tube furnace and Ni-Co/NC at the downstream side. After annealing the sample at 300 °C at the heating rate of 2 °C min^{-1} for 1 h under Ar flow, the resultant NiCoP/NC nanostructures were obatined. The mass loadings of Ni-Co/NC and NiCoP/NC over the Ni-foam current collector in 1 cm^{-1} are 1.4 and 1.5 mg cm^{-2}, respectively.

Materials characterization

The prepared samples were characterized by different characterization techniques. X-ray diffraction (XRD) analysis was performed using the X-ray diffractometer (XRD) with a Cu grid (Rigaku Ultima, λ = 1.54 Å). Raman analysis was carried out using a custom-built Raman spectrometer with a HeNe red laser (632.8 nm) and 1800 lines/mm grating. X-ray photoelectron spectroscopy (XPS) measurements were made using an X-ray photoelectron spectrometer (Thermo Scientific Inc., UK) with Kα radiation ($h\nu$ = 1486.6 eV) to determine the surface oxidation states. The morphology of the samples was characterized using field-emission scanning electron microscopy (JEOL-7800F; JEOL) and transmission electron microscopy (JEM-2010; JEOL). The thermogravimetric analysis (TGA) was performed at a heating rate of 10 °C min^{-1} in Ar atmosphere on an EXSTAR SII TG/DTA 7300 instrument. The specific

surface area and pore size distribution were measured using N_2 adsorption–desorption isotherms using Quantachrome ASiQwin analyzer.

Electrochemical measurements

The electrochemical measurements were performed using an electrochemical workstation ZIVE SP 2 in a three- as well as two-electrode system with 1 M KOH aqueous solution as an electrolyte. Firstly, the electrochemical measurements were performed in a three-electrode system in which Ni-Foam with deposited materials were cut into the 1 cm^2 area and used as working electrodes, platinum wire and Hg/HgO were used as counter and reference electrodes, respectively. To check rate capability, cyclic voltammetry (CV) and galvanostatic charge-discharge (GCD) measurements were performed at different scan rates. The electrochemical impedance spectroscopy (EIS) measurements were conducted in the frequency region of 0.01 Hz to 100 kHz at an open circuit potential of 10 mV.

The two-electrode measurements were performed for aqueous hybrid supercapacitor. The hybrid supercapacitor was fabricated using NiCoP/NC marigold flower as a positive electrode, activated carbon (AC) as a negative electrode and 1 M KOH as an electrolyte. The AC electrode was prepared using following procedure: AC, carbon black (conductive agent) and nafion (as a binder) were mixed in 80:10:10 ratio with ethanol as a solvent to form homogeneous slurry. The obtained slurry was coated on a Ni-foam substrtae and dried at 70 °C for 12 h to form uniform and well-adherent electrode.

The specific capacity (Q_s), specific capacitance (C_S), areal capacitance (C_A), volumetric capacitance (C_V), specific energy and specific power for three-electrode and hybrid supercapacitor were calculated according to the following equations;

$$Q_S = \frac{I \times \Delta t}{m \times 3.6} \quad (1)$$

$$C_S = \frac{I \times \Delta t}{m \times \Delta V} \quad (2)$$

$$C_A = \frac{I \times \Delta t}{A \times \Delta V} \quad (3)$$

$$C_V = \frac{I \times \Delta t}{V \times \Delta V} \quad (4)$$

Where I is the current (A), ΔV is the potential window (V), Δt is the discharge time (s), m is the mass of the active material (mg), A is the area (cm^2) and V is the volume (cm^3) of the device.

The specific energy and specific power of the hybrid device were calculated from the following equations;

$$E = \frac{0.5 \times C_S \times \Delta V^2}{3.6} \quad (5)$$

$$P = \frac{E \times 3600}{\Delta t} \quad (6)$$

Where, E is the specific energy (Wh kg^{-1}) and P is the specific power (W kg^{-1}).

Supporting Information 2

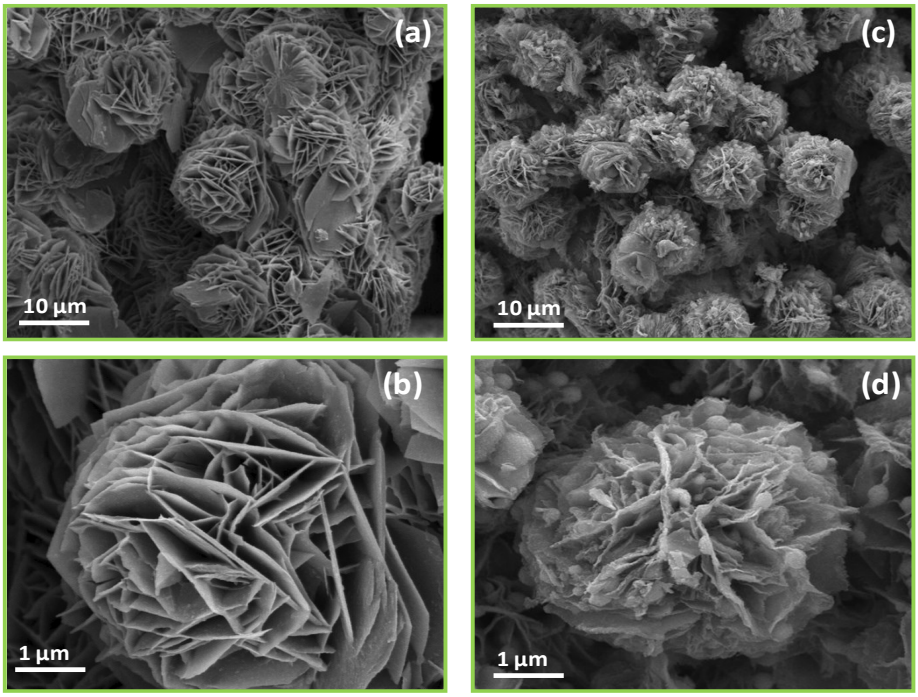

Figure S1 FESEM images of Ni-Co-MOF and Ni-Co/NC nanostructures at two different magnifications.

Supporting Information 3

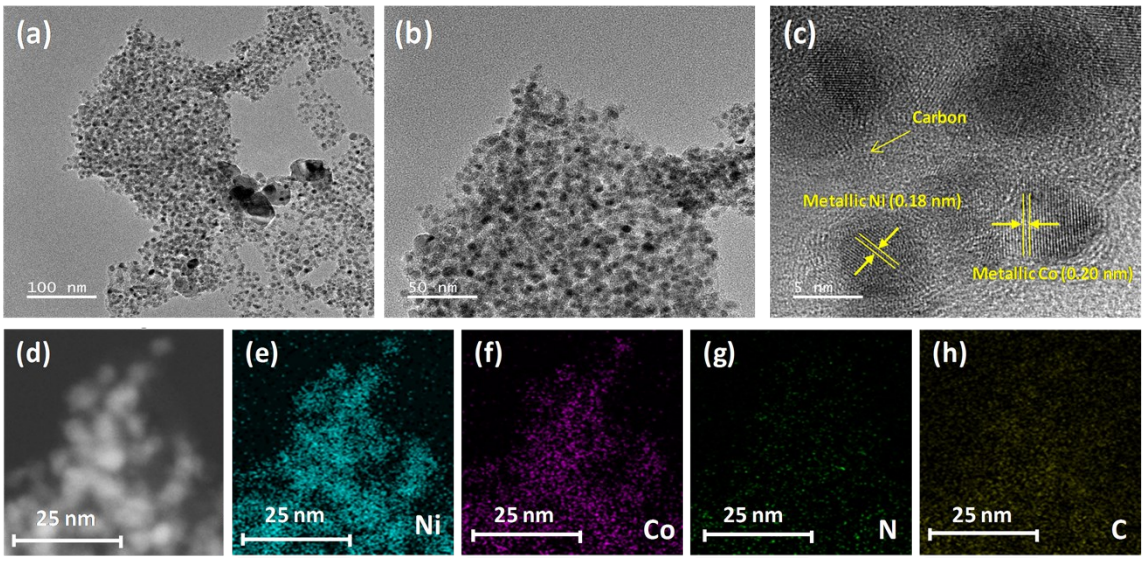

Figure S2 a-c) the TEM images for the Ni-Co/NC hybrid composite and d-h) STEM-EDS elemental mapping images for the Ni-Co/NC hybrid composite.

Supporting Information 4

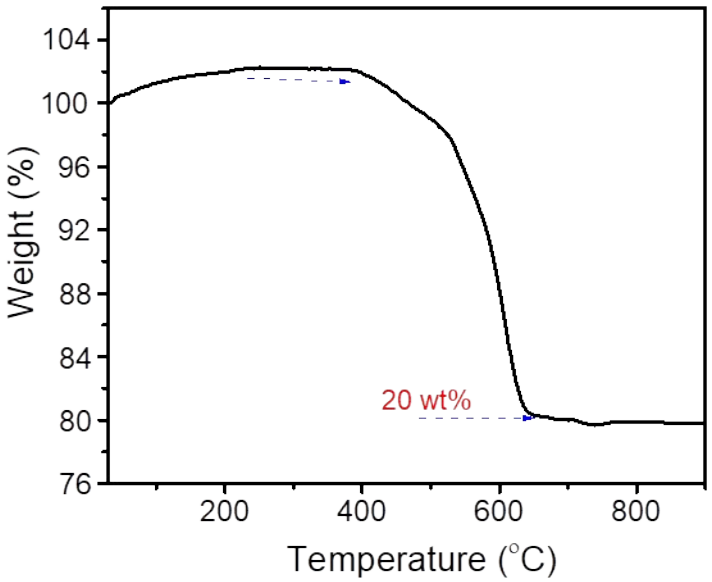

Figure S3 TGA curve of the Ni-Co/NC nanostructures

Supporting Information 5

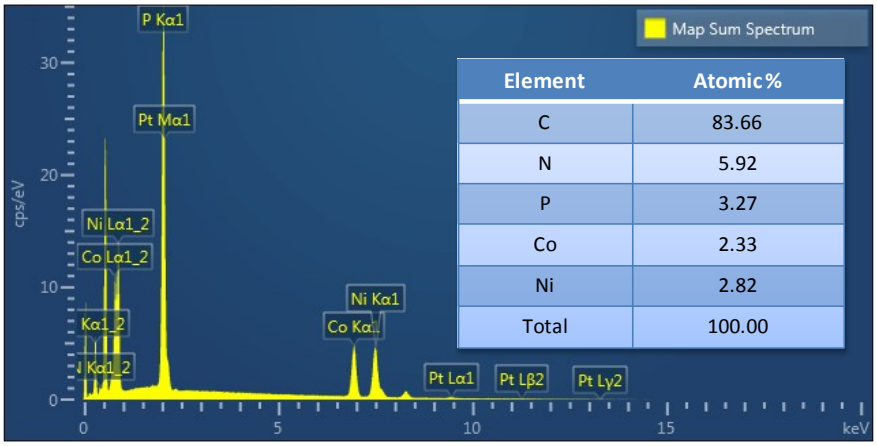

Figure S4 the EDS spectrum from STEM-EDS analysis for the NiCoP/NC marigold flower electrode, inset table shows atomic distribution of elements present in the sample.

Supporting Information 6

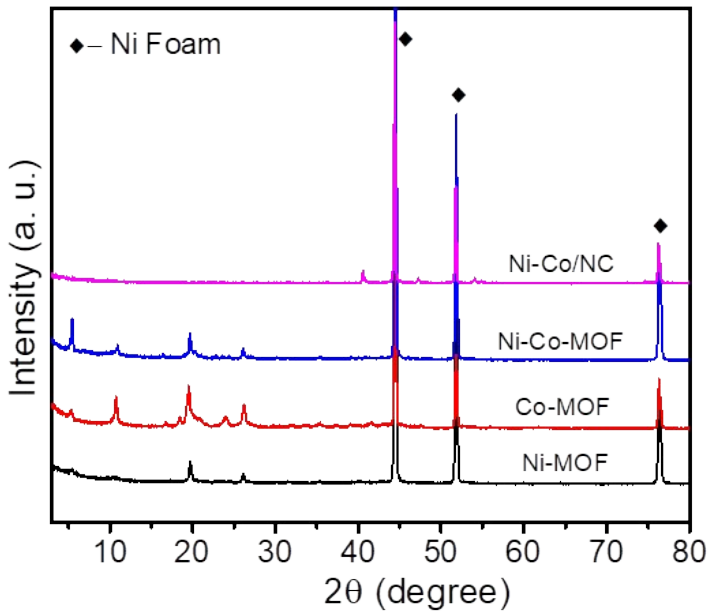

Figure S5 XRD patterns for Ni–MOF, Co–MOF, Ni–Co-MOF and Ni–Co/NC.

Supporting Information 7

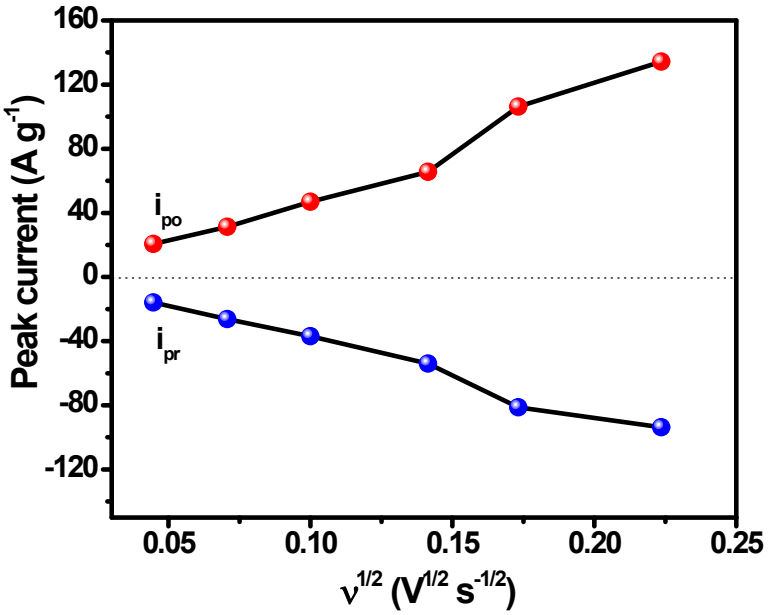

Figure S6 Plot of the anodic and cathodic peak currents against the square root of scan rate.

Supporting Information 8

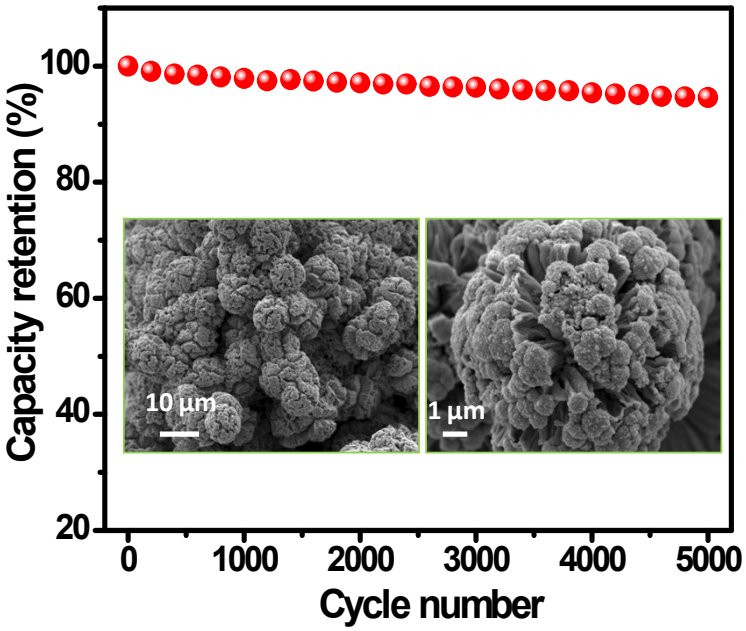

Figure S7 Cycling stability plot of NiCoP/NC. Inset shows post cycling FESEM images of NiCoP/NC nanostructures

Supporting Information 9

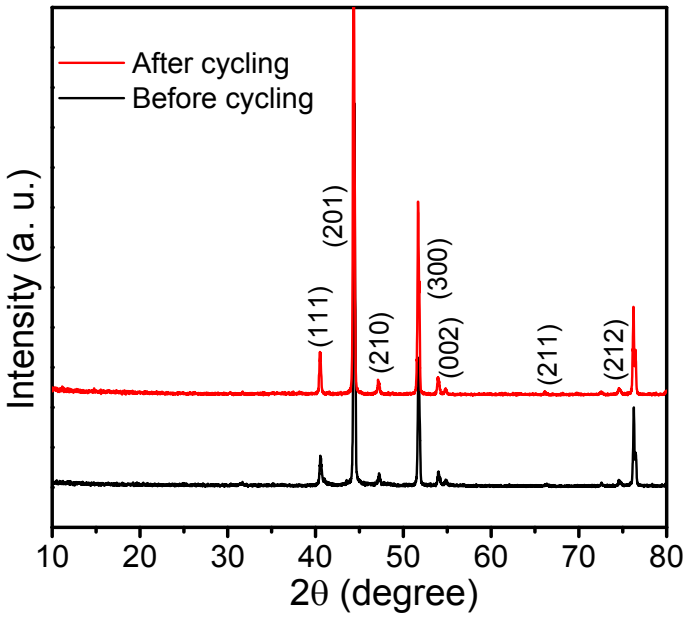

Figure S8 Before and after cycling XRD patterns of NiCoP/NC nanostructures

Supporting Information 10

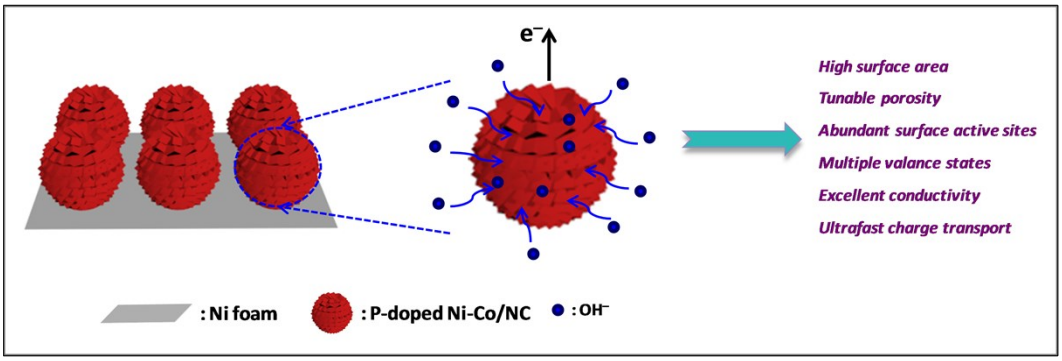

Figure S9 Schematic of the charge intercalation in the NiCoP/NC marigold flower electrode.

Supporting Information 11

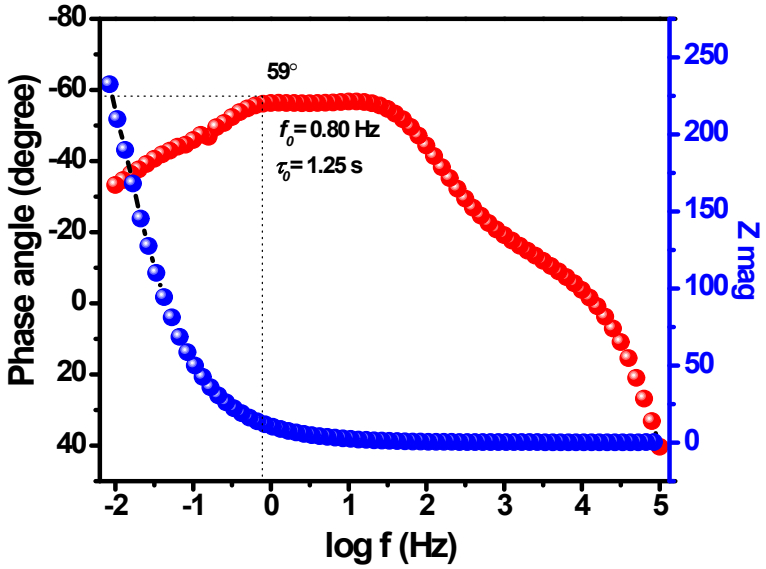

Figure S10 Bode plot for the NiCoP/NC//AC hybrid supercapacitor

Supporting Information 12

Table S1 Comparison of the electrochemical performance of the NiCoP/NC//AC hybrid capacitor with that of similar devices reported in the literature

Device	Specific capacitance	Specific energy; specific power	Cycling stability	Ref.
CoBTC MOF/GNS	183.2 F g^{-1}	49.8 Wh kg^{-1} at 1025.8 W kg^{-1}	92.1% after 5000 cycles	[1]
$ZnCo_2O_4$@$Ni(OH)_2$// AC	112.1 F g^{-1}	40 Wh kg^{-1} at 802.7 W kg^{-1}	98.4% after 5000 cycles	[2]
Co–Mn-MOF//AC	106.7 F g^{-1}	30 Wh kg^{-1} at 685 W kg^{-1}	-	[3]
NiCoS/NC//AC	111. 2 F g^{-1}	39.6 Wh kg^{-1} at 808 W kg^{-1}	81.5% after 3000 cycles	[4]
Co_9S_8/C//AC	166 F g^{-1}	58 Wh kg^{-1} at 1000 W kg^{-1}	90% after 1000 cycles	[5]
Ni-MOF//AC	88 F g^{-1} at 1 A g^{-1}	31.5 Wh kg^{-1} at 800 W kg^{-1}	-	[6]
MnO_2@NiCo-LDH/CoS_2//AC	144.7 F g^{-1} at 0.5 A g^{-1}	49.5 Wh kg^{-1} at 391.5 W kg^{-1}	-	[7]
Co_3O_4@$Co(OH)_2$//AC	131.4 F g^{-1} at 1 A g^{-1}	41.0 Wh kg^{-1} at 1125.9 W kg^{-1}	75% after 10,000 cycles	[8]
NiCoP/NiCo-OH//PC	100 F g^{-1} at 1 A g^{-1}	34 Wh kg^{-1} at 775 W kg^{-1}	92% after 1000 cycles	[9]
Co_3O_4//AC	134 F g^{-1} at 1 A g^{-1}	46.5 Wh kg^{-1} at 790.7 W	86.4% after 8000	[10]

		kg^{-1}	cycles	
NiCoP/NC//AC	172.6 F g^{-1} at 3 A g^{-1}	47 Wh kg^{-1} at 1666 W kg^{-1}	86% after 10,000 cycles	**Present work**

References

[1] N. S. Punde, C. R. Rawool, A. S. Rajpurohit, S. P. Karna, A. K. Srivastava, *ChemistrySelect*, 2018, 3, 11368–11380.

[2] X. Han, Y. Yang, J. J. Zhou, Q. Ma, K. Tao, L. Han, *Chem. Eur. J.,* 2018, 24, 18106–18114.

[3] A. Carton, A. Mesbah, T. Mazet, F. Porcher, M. Francois, *Solid State Sci.,* 2007, 9, 465–471.

[4] M. Yi, C. Zhang, C. Cao, C. Xu, B. Sa, D. Cai, H. Zhan*, Inorg. Chem.,* 2019, 58, 39163924.

[5] S. Sun, J. Luo, Y. Qian, Y. Jin, Y. Liu, Y. Qiu, X. Li, C. Fang, J. Han, Y. Huang, *Adv. Energy Mater.,* 2018, 8, 1801080.

[6] S. W. Gao, Y. W. Sui, F. X. Wei, J. Q. Qi, Q. K. Meng, Y. Z. He, *J. Mater. Sci.,* 2018, 53, 6807–6818.

[7] X. Wang, F. Huang, F. Rong, P. He, R. Que, S. P. Jiang, *J. Mater. Chem. A,* 2019, 7, 12018–12028.

[8] Y. Yang, Q. Ma, L. Han, K. Tao, *Inorg. Chem. Front.,* 2019, 6, 1398–1404.

[9] X. Li, H. Wu, A. M. Elshahawy, L. Wang, S. J. Pennycook, C. Guan, J. Wang, *Adv. Funct. Mater.,* 2018, 28, 1800036.

[10] G. Wei, Z. Zhou, X. Zhao, W. Zhang, C. An, *ACS Appl. Mater. Interfaces,* 2018, 10

, 23721–23730.